Supporting Information for

Secondary organic aerosol formation from reaction of 3-methylfuran with nitrate radicals

Taekyu Joo[1], Jean C. Rivera-Rios[2], Masayuki Takeuchi[3], Matthew J. Alvarado[4], Nga Lee Ng[1,2]

[1]School of Earth and Atmospheric Sciences, Georgia Institute of Technology

[2]School of Chemical and Biomolecular Engineering, Georgia Institute of Technology

[3]School of Civil and Environmental Engineering, Georgia Institute of Technology

[4]Atmospheric and Environmental Research

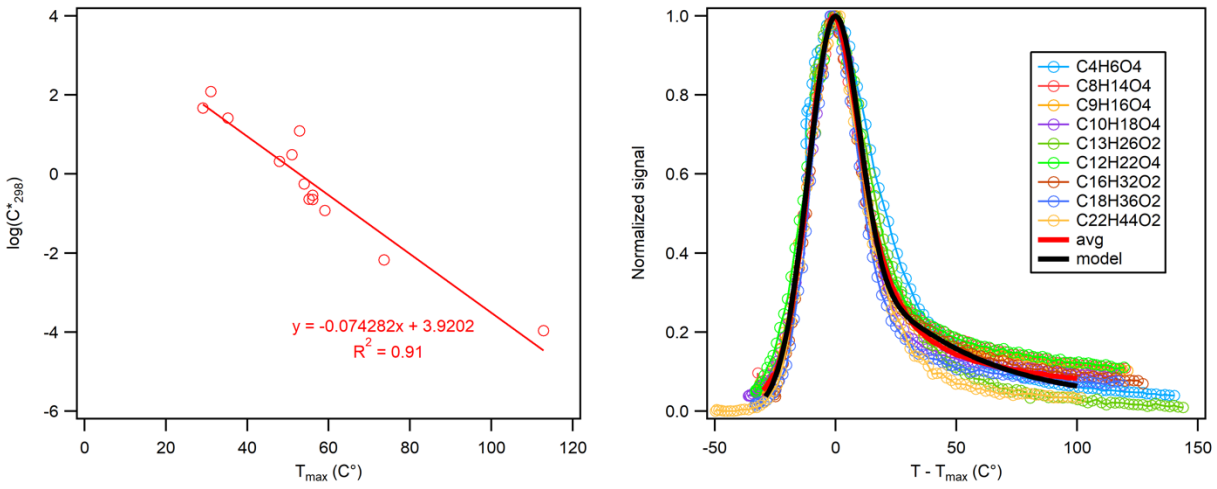

Figure S-1. FIGAERO volatility calibration curve and the shape of fitting curve from the thermograms of calibrants.

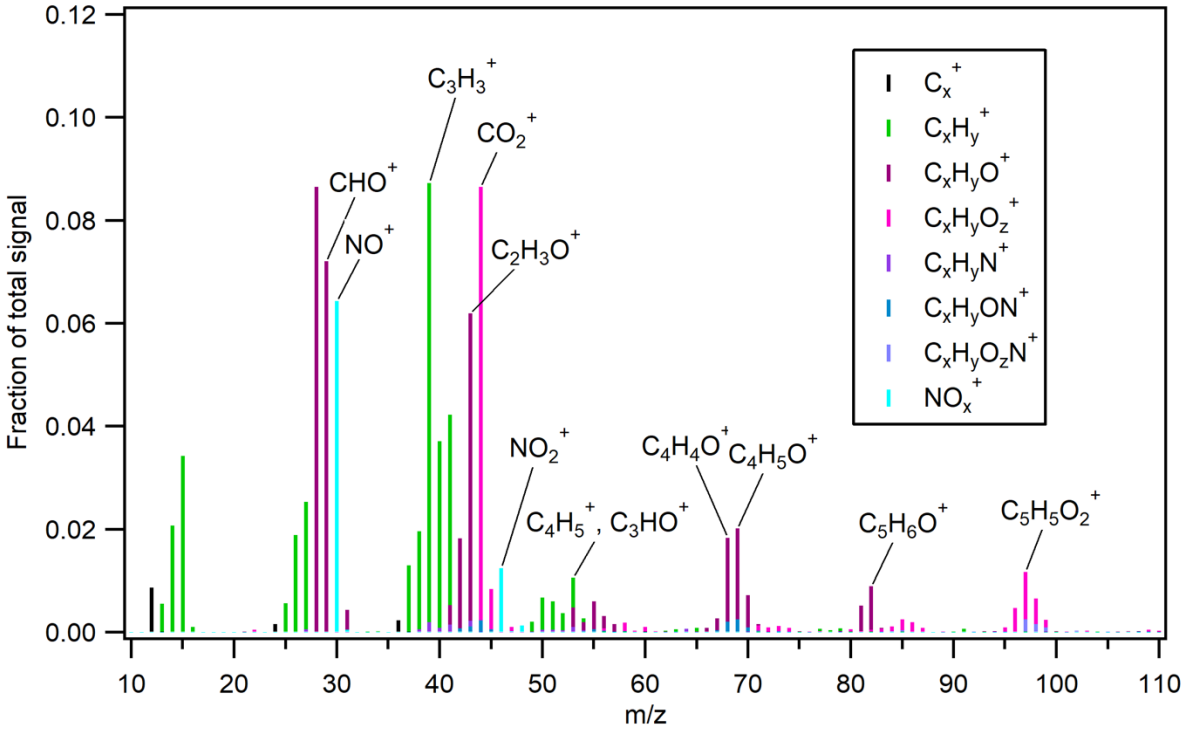

Figure S-2. High-resolution aerosol mass spectrum of the SOA (measured by HR-ToF-AMS) from the 3-methylfuran+NO_3 reaction at peak aerosol growth. The mass spectrum is colored by the ion type to indicate the contribution of each ion type to the mass spectrum. Ions are shown up to *m/z* 110 as the signals beyond this point are negligible.

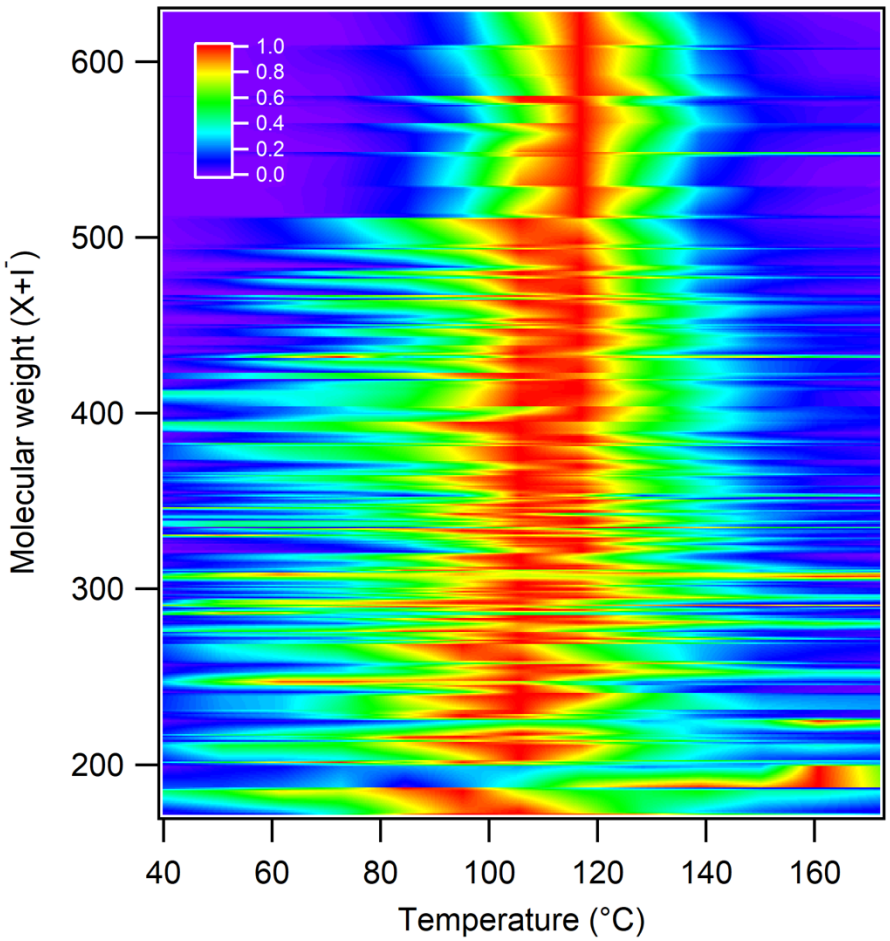

Figure S-3. 2-D thermogram of the SOA from 3-methylfuran+NO_3 reaction at peak aerosol growth.

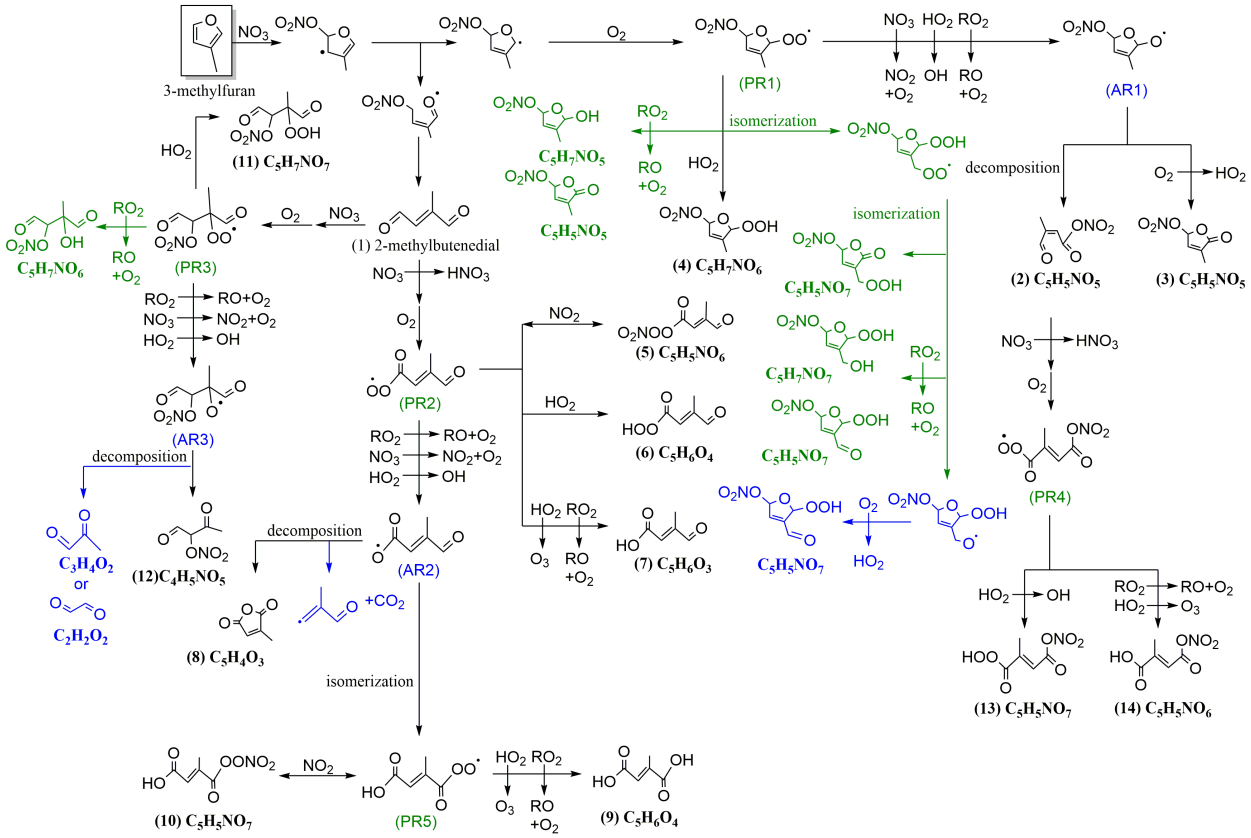

Figure S-4. Proposed mechanism in Figure 5 with peroxy and alkoxy radical highlighted with green and blue, respectively. Colored species are not included in Figure 5 due to the reasons below.

Rates of alkoxy radical decomposition and isomerization are calculated using the structure-activity relationships of Vereecken and Peters[1, 2] and Atkinson.[3] Rates of peroxy radical reactions and the branching ratio are adopted from The Master Chemical Mechanism (MCM v 3.3.1.).[4-7]

Alkoxy radical 1: This secondary alkoxy radical has two decomposition pathways: ring-opened nitrooxy dicarbonyl (compound 2) and cyclic nitrooxy carbonyl (compound 3). Alkoxy radical 1 can react with O_2 to form compound 3 of which decomposition rate is $k_{decomp+O2} = 4.5 \times 10^4\ s^{-1}$. Ring-opening decomposition rate $k_{decomp} = 1.4 \times 10^{10}\ s^{-1}$. Therefore, decomposition to form compound 2 is the more favored pathway.

Alkoxy radical 2: This acyl alkoxy radical can decompose to form compound 8 with O_2 ($k_{decomp+O2} = 4.7 \times 10^4\ s^{-1}$), decompose to form an alkyl radical (number of C = 4) ($k_{decomp} = 5.9 \times 10^5\ s^{-1}$), or isomerize to form PR5 through 1,5-H shift of aldehyde hydrogen ($k_{isom} = 2.7 \times 10^7\ s^{-1}$). We do not include further pathway from the alkyl radical decomposition because the signals of its products are relatively low. Isomerization should dominate because the reaction rate is 2-3 orders of magnitude faster than the decomposition pathways.

Alkoxy radical 3: This tertiary alkoxy radical can decompose to form methylglyoxal and glyoxal ($k_{decomp} = 7.4 \times 10^6\ s^{-1}$) or compound 12 ($k_{decomp} = 3.4 \times 10^8\ s^{-1}$). We show the formation pathway of compound 12 here only (not glyoxal and methylglyoxal) because its pathway would dominate.

Peroxy radical 1: Because this radical can be considered as a secondary peroxy radical, RO_2+RO_2 reaction rate ($k_{secRO2+RO2} = 5.4 \times 10^{-13}$ cm^3 $molecule^{-1}$ s^{-1}) is relatively slower compared to the other reaction channel such as RO_2+HO_2 ($k_{RO2+HO2} = 2.3 \times 10^{-11}$ cm^3 $molecule^{-1}$ s^{-1}) or RO_2+NO_3 ($k_{RO2+NO3} = 2.3 \times 10^{-12}$ cm^3 $molecule^{-1}$ s^{-1}). NO_3 radical concentration is estimated to be 4.9×10^7 molecule cm^{-3} based on the rate of decay of furan compounds measured by GC-FID. If we assume RO_2 and HO_2 concentrations to be similar to NO_3, PR1 would preferentially react with either HO_2 or NO_3 because the lifetime of peroxy radical would be shorter (reaction rate will be around 2-4 orders of magnitude faster compared to the RO_2+RO_2 reaction channel). The isomerization of PR1 is difficult to estimate but has the potential to be fast based on similar systems (i.e. HPALD).[8] However, the temporal profiles of products from isomerization pathway ($C_5H_5NO_7$ and $C_5H_7NO_7$) show that these species are formed as later-generation compounds instead. Therefore, we do not consider isomerization and RO_2+RO_2 reaction in Figure 5.

Peroxy radicals 2, 4, 5: If we apply $k_{RO2+NO3} = 2.3 \times 10^{-12}$ cm^3 $molecule^{-1}$ s^{-1}, $k_{RO2+HO2} = 1.4 \times 10^{-11}$ cm^3 $molecule^{-1}$ s^{-1}, $k_{RO2+NO2} = 9.0 \times 10^{-12}$ cm^3 $molecule^{-1}$ s^{-1}, and $k_{acylRO2+RO2} = 1.7 \times 10^{-11}$ cm^3 $molecule^{-1}$ s^{-1}, all products from PR2 show comparable time scale. Unlike PR1, PR2 is an acylperoxy radical which is reported to have the fastest RO_2+RO_2 reaction rate. NO_2 reaction channel is excluded for PR4 because the compounds with two -ONO_2 functional group are detected to be minor. Peroxide from PR5+HO_2 reaction is also a minor compound.

Peroxy radical 3: Because PR3 is a tertiary RO_2, reaction rate is the slowest among RO_2+RO_2 reaction ($k_{terRO2+RO2} = 5.7 \times 10^{-11}$ cm^3 $molecule^{-1}$ s^{-1}). The formation of $C_5H_7NO_6$ via RO_2+RO_2 is very unlikely to proceed compared to AR3 formation.

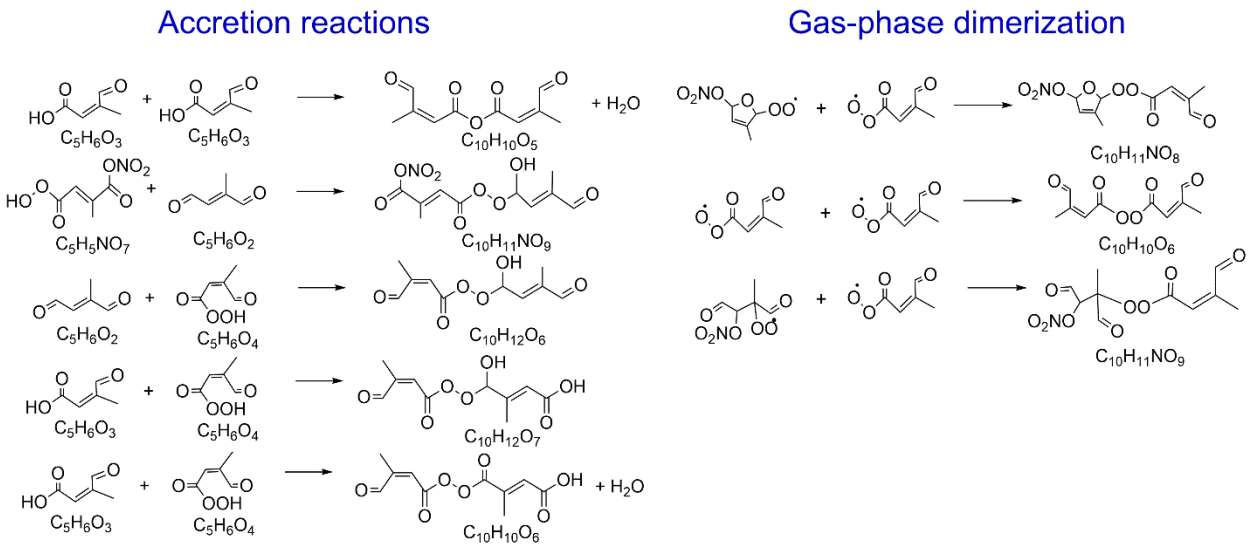

Figure S-5. Possible particle-phase accretion reactions and gas-phase RO_2+RO_2 dimerization. Proposed peroxyhemiacetal formation, esterification reactions,[9, 10] and ROOR' formation from RO_2+RO_2 reaction can form selected C_{10} compounds in Figure 2.[11-14]

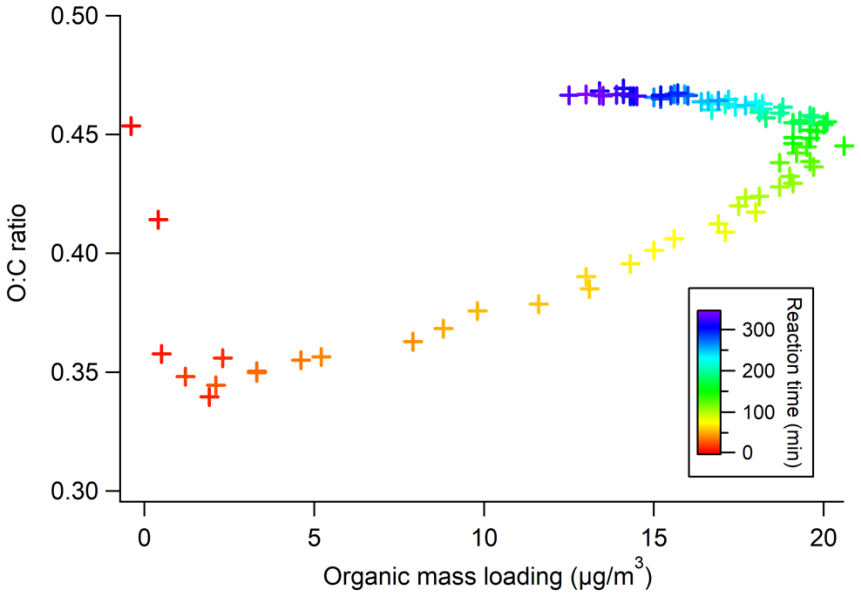

Figure S-6. Variation of O/C ratio as a function of organic mass loading measured by the HR-ToF-AMS.

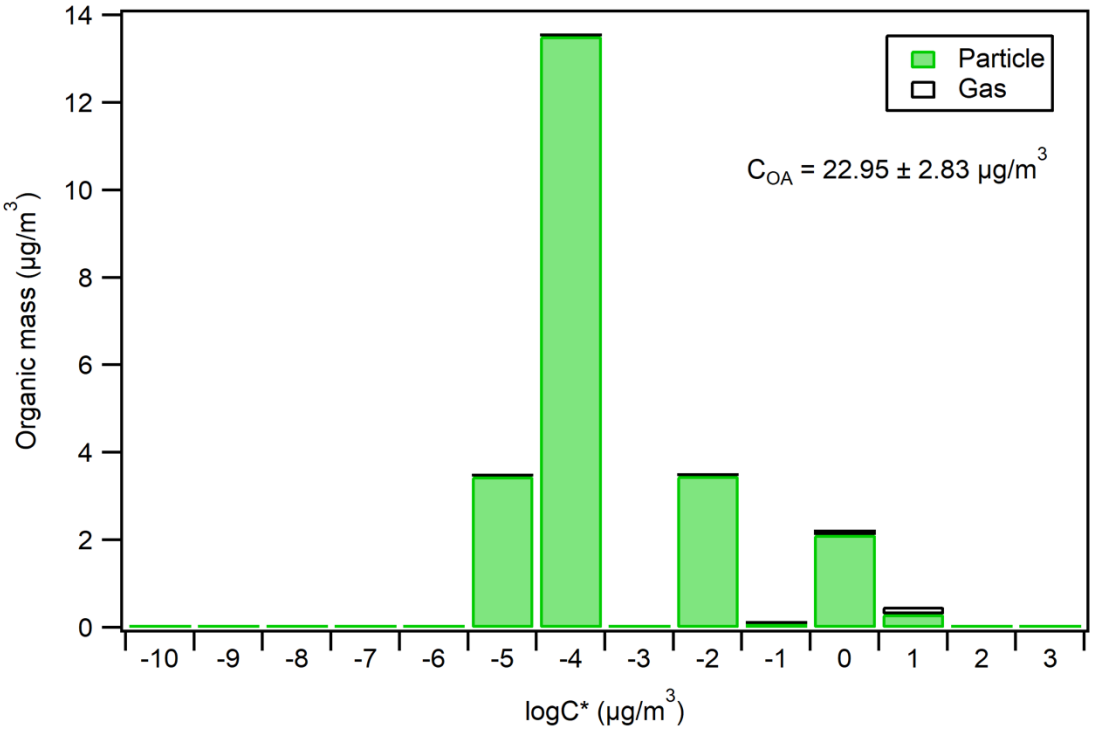

Figure S-7. Organic mass concentration of each volatility bin at peak aerosol growth for Experiment #2 in Table 1 (3-methylfuran: 328 ppb, i.e., 1103 µg m^{-3}). FIGAERO-HR-ToF-CIMS signal is converted into mass concentration by assuming the observed signal is equal to the organic mass measured by the HR-ToF-AMS. Organic concentration reported from the HR-ToF-AMS has been corrected for particle collection efficiency (by converting AMS organic and inorganic measurements to volume and comparing this to the SMPS volume). Sensitivity difference to I^- for each species is not considered here. Green bar indicates the condensed-phase mass concentration and transparent bar indicates the estimated gas-phase mass concentration.

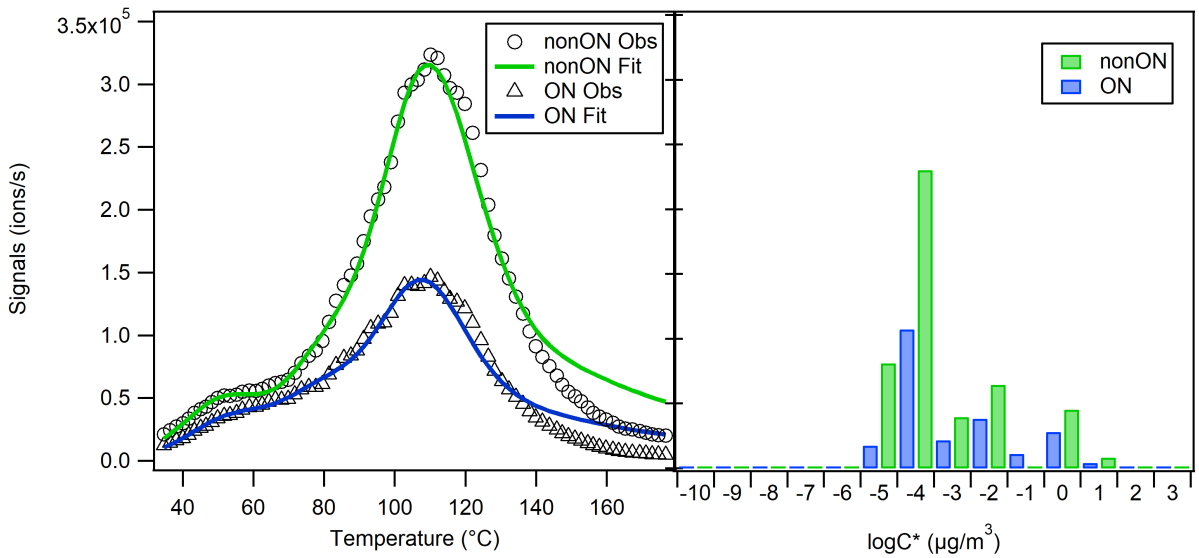

Figure S-8. Left panel shows thermograms of non-nitrate organics (nonON) and particulate organic nitrates (ON) measured by FIGAERO-HR-ToF-CIMS for a typical experiment (Experiment #2 in Table 1). Signals at t = 140 min and t = 200 min are averaged here because particle organic nitrates reach the maximum at t = 200 min. Volatility bins expressed as saturation mass concentration are estimated following the method in Stark et al.[15]

Table S-1. Mass concentration of each volatility bin in Figure S-7.

C* (µg m^{-3})	10^{-5}	10^{-4}	10^{-3}	10^{-2}	10^{-1}	1	10
Particle (µg m^{-3})	3.45	13.52	0	3.47	0.09	2.12	0.30
Total (µg m^{-3})	3.45	13.52	0	3.47	0.09	2.24	0.48

References

(1) Vereecken, L.; Peeters, J. Decomposition of substituted alkoxy radicals—part I: a generalized structure–activity relationship for reaction barrier heights. *Physical Chemistry Chemical Physics* **2009,** *11* (40), 9062-9074.
(2) Vereecken, L.; Peeters, J. A structure–activity relationship for the rate coefficient of H-migration in substituted alkoxy radicals. *Physical Chemistry Chemical Physics* **2010,** *12* (39), 12608-12620.
(3) Atkinson, R. Rate constants for the atmospheric reactions of alkoxy radicals: An updated estimation method. *Atmospheric Environment* **2007,** *41* (38), 8468-8485.
(4) Jenkin, M.; Saunders, S.; Wagner, V.; Pilling, M. Protocol for the development of the Master Chemical Mechanism, MCM v3 (Part B): tropospheric degradation of aromatic volatile organic compounds. *Atmospheric Chemistry and Physics* **2003,** *3* (1), 181-193.
(5) Jenkin, M. E.; Saunders, S. M.; Pilling, M. J. The tropospheric degradation of volatile organic compounds: a protocol for mechanism development. *Atmospheric Environment* **1997,** *31* (1), 81-104.
(6) Saunders, S. M.; Jenkin, M. E.; Derwent, R.; Pilling, M. Protocol for the development of the Master Chemical Mechanism, MCM v3 (Part A): tropospheric degradation of non-aromatic volatile organic compounds. *Atmospheric Chemistry and Physics* **2003,** *3* (1), 161-180.
(7) Saunders, S. M.; Pascoe, S.; Johnson, A. P.; Pilling, M. J.; Jenkin, M. E. Development and preliminary test results of an expert system for the automatic generation of tropospheric VOC degradation mechanisms. *Atmospheric Environment* **2003,** *37* (13), 1723-1735.
(8) Teng, A. P.; Crounse, J. D.; Wennberg, P. O. Isoprene peroxy radical dynamics. *Journal of the American Chemical Society* **2017,** *139* (15), 5367-5377.
(9) Kroll, J. H.; Seinfeld, J. H. Chemistry of secondary organic aerosol: Formation and evolution of low-volatility organics in the atmosphere. *Atmospheric Environment* **2008,** *42* (16), 3593-3624.
(10) Ziemann, P. J.; Atkinson, R. Kinetics, products, and mechanisms of secondary organic aerosol formation. *Chemical Society Reviews* **2012,** *41* (19), 6582-6605.
(11) Kwan, A.; Chan, A.; Ng, N.; Kjærgaard, H. G.; Seinfeld, J.; Wennberg, P. Peroxy radical chemistry and OH radical production during the NO 3-initiated oxidation of isoprene. *Atmospheric Chemistry and Physics* **2012,** *12* (16), 7499-7515.
(12) Kan, C. S.; Calvert, J. G.; Shaw, J. H. Reactive channels of the methyldioxy-methyldioxy reaction. *The Journal of Physical Chemistry* **1980,** *84* (25), 3411-3417.
(13) Niki, H.; Maker, P.; Savage, C.; Breitenbach, L. Fourier-transform infrared studies of the self-reaction of CH3O2 radicals. *The Journal of Physical Chemistry* **1981,** *85* (7), 877-881.
(14) Tyndall, G.; Cox, R.; Granier, C.; Lesclaux, R.; Moortgat, G.; Pilling, M.; Ravishankara, A.; Wallington, T. Atmospheric chemistry of small organic peroxy radicals. *Journal of Geophysical Research: Atmospheres* **2001,** *106* (D11), 12157-12182.
(15) Stark, H.; Yatavelli, R. L.; Thompson, S. L.; Kang, H.; Krechmer, J. E.; Kimmel, J. R.; Palm, B. B.; Hu, W.; Hayes, P. L.; Day, D. A.; Campuzano-Jost, P.; Canagaratna, M. R.; Jayne, J. T.; Worsnop, D. R.; Jimenez, J. L. Impact of thermal decomposition on thermal desorption instruments: advantage of thermogram analysis for quantifying volatility distributions of organic species. *Environmental Science & Technology* **2017,** *51* (15), 8491-8500.